Crystal Structures of Fructose 1,6-Bisphosphatase: Mechanism of Catalysis and Allosteric Inhibition Revealed in Product Complexes[†,‡]

Jun-Yong Choe, Herbert J. Fromm, and Richard B. Honzatko*

Department of Biochemistry, Biophysics, and Molecular Biology, Iowa State University, Ames, Iowa 50011

Received March 13, 2000; Revised Manuscript Received May 10, 2000

ABSTRACT: Crystal structures of metal−product complexes of fructose 1,6-bisphosphatase (FBPase) reveal competition between AMP and divalent cations. In the presence of AMP, the Zn^{2+}−product and Mg^{2+}−product complexes have a divalent cation present only at one of three metal binding sites (site 1). The enzyme is in the T-state conformation with a disordered loop of residues 52−72 (loop 52−72). In the absence of AMP, the enzyme crystallizes in the R-state conformation, with loop 52−72 associated with the active site. In structures without AMP, three metal-binding sites are occupied by Zn^{2+} and two of three metal sites (sites 1 and 2) by Mg^{2+}. Evidently, the association of AMP with FBPase disorders loop 52−72, the consequence of which is the release of cations from two of three metal binding sites. In the Mg^{2+} complexes (but not the Zn^{2+} complexes), the 1-OH group of fructose 6-phosphate (F6P) coordinates to the metal at site 1 and is oriented for a nucleophilic attack on the bound phosphate molecule. A mechanism is presented for the forward reaction, in which Asp74 and Glu98 together generate a hydroxide anion coordinated to the Mg^{2+} at site 2, which then displaces F6P. Development of negative charge on the 1-oxygen of F6P is stabilized by its coordination to the Mg^{2+} at site 1.

Fructose 1,6-bisphosphatase (FBPase,[1] EC 3.1.3.11) hydrolyzes fructose 1,6-bisphosphate ($F16P_2$) to fructose 6-phosphate (F6P) and phosphate (P_i) (*1*−*6*). The enzyme plays a central role in gluconeogenesis, and is inhibited allosterically by AMP, the binding of which is cooperative with a Hill coefficient of 2 (*7*−*9*). Fructose 2,6-bisphosphate ($F26P_2$), which binds with high affinity to the active site, inhibits FBPase synergistically with AMP (*10*−*12*). FBPase requires divalent cations (Mg^{2+}, Mn^{2+}, and/or Zn^{2+}) for activity, and certain monovalent cations (K^+, NH_4^+, and Tl^+) further enhance catalysis (*3*, *5*, *13*). Enzyme activity increases sigmoidally as a function of divalent cation concentration at pH 7.5 (Hill coefficient of approximately 2), but at pH 9.6, the variation is hyperbolic (*8*, *14*).

The mammalian enzyme is a homotetramer (Figure 1), which exists in distinct conformational states, depending on the relative concentrations of active site ligands and AMP (*15*). In the absence of AMP, FBPase, with or without metal cofactors and/or other active site ligands, is in its R-state. In the presence of AMP, however, the top pair of subunits rotates 17° relative to the bottom pair, resulting in the T-state conformer. The minimum distance separating AMP molecules from any given active site is approximately 30 Å (*16*, *17*). Yet on the basis of kinetics, NMR, and fluorescence studies, the binding of AMP and Mg^{2+} is mutually exclusive (*11*, *18*, *19*).

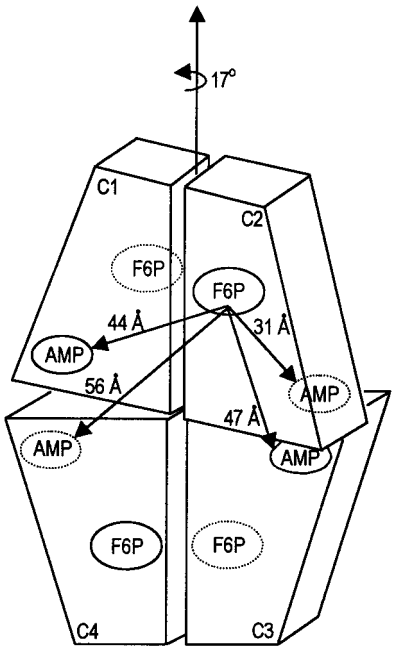

FIGURE 1: Schematic of the T-state conformation of FBPase. A rotation of the subunit pair C1−C2 by 17° as shown transforms the T-state into the R-state conformer. Dotted ovals represent ligand binding sites on faces of the tetramer hidden from view. Distances measured from atom C-2 of F6P of subunit C2 to atoms C-1′ of four bound AMP molecules are presented.

[†] This work was supported in part by National Institutes of Health Research Grant NS-10546 and National Science Foundation Grant MCB-9603595. This is Journal Paper J-18833 of the Iowa Agriculture and Home Economics Experiment Station, Ames, Project 3191, and is supported by Hatch Act and State of Iowa funds.

[‡] Coordinates and structure factors (codes 1cnq, 1eyi, 1eyj, and 1eyk) for the structures described in this paper have been deposited with the Protein Data Bank, Research Collaboratory for Structural Bioinformatics (RCSB), http://www.rcsb.org/pdb/.

* Corresponding author. Telephone: (515) 294-6116. Fax: (515) 294-0453. E-mail: honzatko@iastate.edu.

[1] Abbreviations: FBPase, fructose 1,6-bisphosphatase; P_i, phosphate; F6P, fructose 6-phosphate; $F16P_2$, fructose 1,6-bisphosphate; $F26P_2$, fructose 2,6-bisphosphate; 2,5-AnG-1,6-P_2, 2,5-anhydroglucitol 1,6-bisphosphate; SDS−PAGE, sodium dodecyl sulfate−polyacrylamide gel electrophoresis.

10.1021/bi000574g CCC: $19.00
Published on Web 06/24/2000

In published crystal structures, however, the number of metal cations bound to the active site is insensitive to the state of ligation of the AMP site. Two Mn^{2+} or two Zn^{2+} ions bind to the active site in the presence or absence of AMP (*20*, *21*). Mn^{2+} association at site 2 is evidently weaker in FBPase complexes with AMP relative to those without AMP (*21*), but the conformational changes in FBPase which cause metal−AMP competition are unsettled. Weaker metal binding to site 2 may arise from the relative rotation of the two folding domains of the FBPase subunit (*21*). Choe et al. (*23*), however, in a Zn^{2+}−product complex of FBPase find little support for rigid body rotations of domains within subunits of FBPase. On the other hand, in that same complex, loop 52−72 associates with an active site that includes three zinc cations. Asp68 of the loop coordinates directly to the Zn^{2+} at metal site 3, and all Zn^{2+} ions are bound firmly to the enzyme, as evidenced by their low thermal parameters. Hence, Choe et al. (*23*) propose an alternative mechanism, in which FBPase has an ordered loop in the active R-state with three bound metals and a disordered loop in the T-state with significantly reduced affinity for metal cations. Yet to be demonstrated, however, is whether AMP, by binding to its allosteric site, displaces loop 52−72 and/or metals from the active site of metal−product complexes of FBPase.

Presented here are crystallographic structures of product complexes of recombinant porcine FBPase in the presence and absence of AMP. In the absence of AMP, FBPase is in the R-state and loop 52−72 associates with the active site, whereas in the presence of AMP, the enzyme crystallizes in the T-state with a disordered loop. The products (F6P and P_i) are present in crystal structures with and without AMP, but metal ligation of the active site differs significantly. In the absence of AMP, Zn^{2+} binds to all three metal sites and Mg^{2+} to two of three metal sites, whereas in the presence of AMP, divalent cations (either Zn^{2+} or Mg^{2+}) bind to a single common site. Furthermore, in only the Mg^{2+} complexes, the 1-OH group of F6P directly coordinates to the metal at site 1, suggesting a direct role for that metal in the catalytic mechanism of FBPase.

EXPERIMENTAL PROCEDURES

Expression and Purification of Wild-Type FBPase. FBPase-deficient *Escherichia coli* strain DF657 [*tonA22, ompF627(T2R), relA1, pit10, spoT1,* Δ*(fbp)287*; Genetic Stock Center at Yale University, New Haven, CT] was used in the expression of recombinant wild-type porcine FBPase. Expression and purification of FBPase followed the procedures of Burton et al. (*24*) with minor modification. After centrifugation to remove cell debris, the supernatant fluid was subjected to heat treatment, centrifugation, volume reduction of the supernatant by pressure concentration through an Amicon PM-30 membrane, and then CM-Sepharose column chromatography. FBPase eluted as a single peak, using a NaCl gradient (from 20 to 400 mM) in 10 mM Tris-malonate (pH 6.0).

Crystallization of the Product Complex. Crystals of FBPase were grown by the method of hanging drops. Crystals of T-state complexes grew from equal parts of a protein solution [10 mg/mL FBPase, 10 mM KP_i (pH 7.4), 2 mM $ZnCl_2$ or 5 mM $MgCl_2$, 5 mM F6P, and 5 mM AMP] and a precipitant solution [100 mM Hepes (pH 7.0) and 10% (w/v) polyethylene glycol 3350]. Crystals of R-state complexes grew from equal parts of a protein solution [10 mg/mL FBPase, 10 mM KP_i (pH 7.4), 5 mM $ZnCl_2$ or 5 mM $MgCl_2$, and 5 mM F6P] and a precipitant solution [2.5 mM Tris-malonate (pH 7.4) and 6% (w/v) polyethylene glycol 3350]. The droplet volume was 4 μL. Wells contained 500 μL of the precipitant solution. Crystals with dimensions of 0.4 mm × 0.4 mm × 0.3 mm grew in approximately 3 days at 4 and 37 °C. Structures of crystals grown at 37 and 4 °C are identical. Data presented below are from crystals grown at 37 °C.

Data Collection. Data were collected at Iowa State University on a rotating anode/Siemens area detector at 120 K, using CuKα radiation passed through a graphite monochromator. Data were reduced by XENGEN (*25*).

Structure Determination, Model Building, and Refinement. Crystals grown for this study are isomorphous to either the Zn^{2+}−product complex (*23*) or AMP complexes reported by Lipscomb and co-workers (*16*). Phase angles, used in the generation of initial electron density maps, were based on models from which water molecules, metal cations, small-molecule ligands, and residues 52−72 had been omitted. Residues 52−72 were built into the electron density of omit maps, with reference to the C^α coordinates of loop 52−72 from the Zn^{2+}−product complex (*23*), using the program XTALVIEW (*26*) and a Silicon Graphics workstation (Indigo2). Added to the single independent subunit of crystals grown in the absence of AMP were two molecules of P_i (active site and AMP site), one molecule of F6P (active site), and either three zinc or two magnesium cations (active site). Subunits of crystals grown in the presence of AMP each had one molecule of P_i, F6P, and AMP, and one metal cation (either Mg^{2+} or Zn^{2+}). Two models were generated for all complexes, which differed in the choice of F6P anomer (α or β). The resulting models underwent refinement using CNS (*27*) with force constants and parameters of stereochemistry from Engh and Huber (*28*). A cycle of refinement consisted of slow cooling from 2500 to 300 K in steps of 25 K, followed by 120 cycles of conjugate gradient minimization, and concluded by the refinement of individual *B*-parameters. *B*-Parameter refinement employed restraints of 1.5 Å^2 on nearest neighbor and next-to-nearest neighbor main chain atoms, 2.0 Å^2 on nearest neighbor side chain atoms, and 2.5 Å^2 on next-to-nearest neighbor side chain atoms.

In subsequent cycles of refinement, water molecules were fit to a difference electron density of 2.5σ or better and were added until no significant decrease was evident in the R_{free} value. Included in the final model were water molecules which make suitable donor−acceptor distances with respect to each other and the protein, and have *B*-parameters of <65 Å^2.

RESULTS

General Features of Metal−Product Complexes of FBPase. Recombinant wild-type FBPase that is used here is free of proteolysis, and is greater than 95% pure on the basis of SDS−PAGE (data not shown).

Crystals grown in the presence of AMP belong to space group $P2_12_12$ (Zn^{2+} complex, $a = 60.12$ Å, $b = 166.14$ Å, and $c = 79.53$ Å; Mg^{2+} complex, $a = 59.86$ Å, $b = 165.82$ Å, and $c = 79.51$ Å), and are isomorphous with respect to those reported by Lipscomb and co-workers (*16*). Two

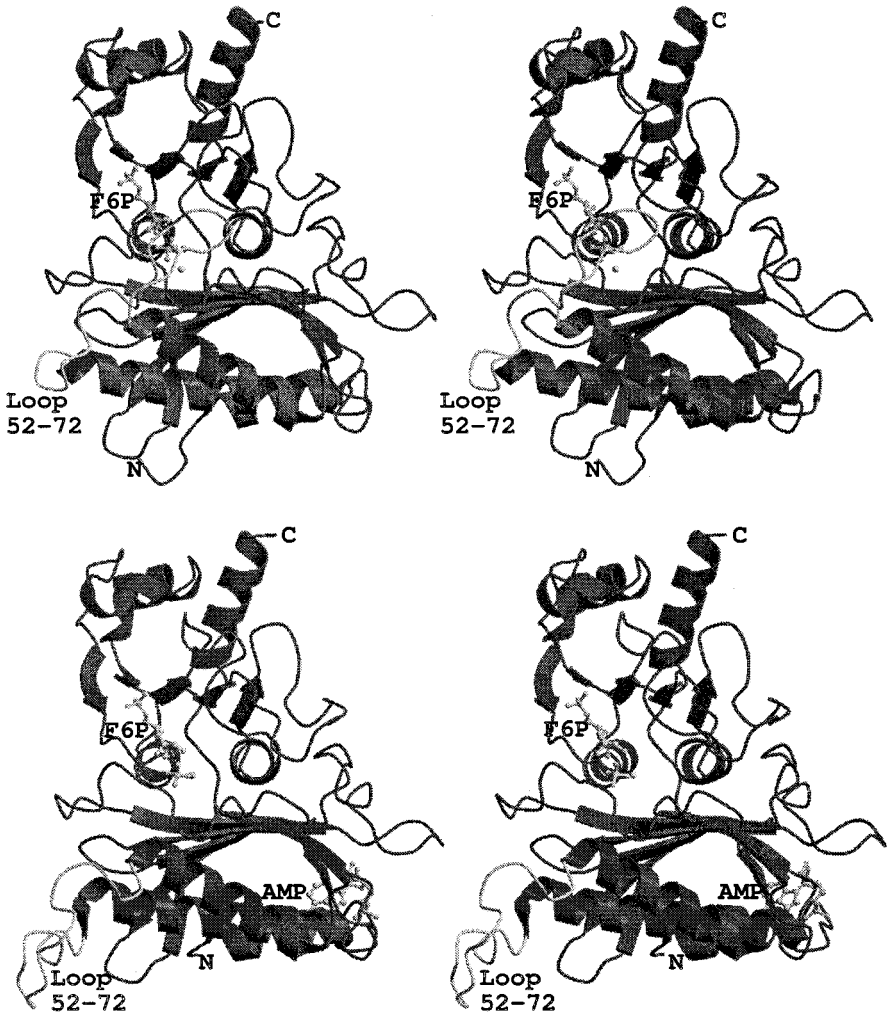

FIGURE 2: Stereoviews of a single FBPase subunit in the T- and R-states. The subunit here is in the orientation of subunit C2 of Figure 1. Loop 52−72 is engaged with the active site (top), whereas loop 52−72 is disengaged from the active site in the T-state (bottom). Residues 63−70 of the T-state are known only approximately from crystal structures. This figure is drawn with MOLSCRIPT (*38*) and RASTER3D (*39*).

subunits of FBPase are in the asymmetric unit of this crystal form. C^{α} coordinates of the independent subunits superimposed (excluding residues 63−70) with a root-mean-square deviation of 0.20 Å. The two subunits are identical to within experimental uncertainty. As noncrystallographic restraints were not used in the refinement, the deviation reported above is a reasonable estimate of coordinate uncertainty. The enzyme is in the canonical T-state (*16*). AMP occupies the allosteric pocket, and P_i, F6P, and one metal cation (either Zn^{2+} or Mg^{2+}) occupy the active site (Figure 2). Regions of weak or absent electron density include residues 1−8 and 63−70. The model begins at residue 9 and continues to the last residue of the sequence, but residues 63−70 are unreliable, as evidenced by high thermal parameters. When residues 63−70 are excluded, thermal parameters vary from 5 to 52 $Å^2$.

Crystals grown in the absence of AMP belong to space group *I*222 (Zn^{2+} complex, $a = 52.34$ Å, $b = 82.82$ Å, and $c = 165.77$ Å; Mg^{2+} complex, $a = 52.12$ Å, $b = 82.51$ Å, and $c = 165.49$ Å). Failure to detect systematic absences, because of an error in a commercial software package, led to the initial space group assignment of $P2_12_12$ ($a = 52.34$ Å, $b = 165.77$ Å, and $c = 82.82$ Å), reported by Choe et al. (*23*). Evaluation of the packing of FBPase tetramers and inspection of the data clearly indicate the higher-symmetry space group. The Zn^{2+}−product structure reported by Choe et al. (*23*) is not changed, but the statistics of refinement (due to the rejection of systematic absences) are much improved in the new space group. The enzyme is in the R-state, but has an ordered loop 52−72, associated with the active site (Figure 2). P_i occupies the allosteric pocket, binding to the 5′-phosphoryl site of AMP, and P_i, F6P, and either two Mg^{2+} or three Zn^{2+} ions occupy the active site. The model begins at residue 7, with weak or absent electron density for residues 1−6 and 22−25. When these regions of weak or absent electron density are excluded, thermal parameters vary from 5 to 67 $Å^2$. Conformational differences relevant to the structure and function of FBPase are discussed below.

Statistics for data collection and refinement for all the structures are given in Table 1. Uncertainty in coordinates is approximately 0.25 Å. The models have stereochemistry generally better than what is typical for structures of a nominal resolution of 2.0 Å, as determined by PROCHECK (*29*).

Metal−Product Complexes of FBPase in the T-State. In the presence of AMP, the Mg^{2+}−product and Zn^{2+}−product complexes adopt identical global conformations, similar to

Table 1: Statistics of Data Collection and Refinement

	R-state Zn^{2+}	R-state Mg^{2+}	T-state Zn^{2+}	T-state Mg^{2+}
resolution limit (Å)	2.27	2.32	2.23	2.28
no. of reflections	72666	72680	119374	122394
no. of unique reflections	15519	15014	36815	35127
completeness (%) of data set	99	99	99	99
completeness (%) of last shell (approximately 2.3−2.4 Å)	90	96	94	95
R_{sym}[a]	0.055	0.078	0.106	0.083
no. of reflections used in refinement[b]	12016	11506	27861	27847
no. of atoms[c]	2749	2718	5473	5512
no. of solvent sites	194	164	389	428
R-factor[d]	0.170	0.187	0.217	0.197
R_{free}[e]	0.220	0.238	0.271	0.255
mean *B* (Å^2)				
protein	16	22	24	21
active site ligands (F6P/P_i/metals)	7/9/17	19/35/21	17/29/19	18/51/22
allosteric site ligands (AMP or P_I)	33	39	26	17
root-mean-square deviations				
bond lengths (Å)	0.005	0.006	0.007	0.007
bond angles (deg)	1.30	1.31	1.36	1.34
dihedral angles (deg)	23.2	22.9	23.8	23.6
improper dihedral angles (deg)	0.77	0.76	0.81	0.80

[a] $R_{sym} = \Sigma_j\Sigma_i|I_{ij} - \langle I_j\rangle|/\Sigma_j\Sigma_i I_{ij}$, where *i* runs over multiple observations of the same intensity and *j* runs over all crystallographically unique intensities. [b] All reflections from 5 to 2.27 Å and $F_{obs} > 0$ not used in the calculation of R_{free}. [c] Includes hydrogen atoms linked to polar atoms. [d] *R*-factor $= \Sigma|F_{obs} - F_{calc}|/\Sigma F_{obs}$, where $F_{obs} > 0$. [e] *R*-factor based upon 10% of the data randomly chosen and not used in refinement.

T-state structures of FBPase reported by other investigators (*16*, *30*−*32*). Nonetheless, the structures here represent the first instances of product complexes of FBPase in the T-state, and as such are necessary complements to product complexes of FBPase in the R-state.

In the T-state, AMP binds to the allosteric pocket, and is covered by strong electron density. The AMP molecule is in the anti conformation ($\chi = -166°$), with a 3′-endo ribosyl group (a pseudo puckering angle of 9°), and an O5′−C5′−C4′−C3′ torsion angle (γ) of 56°. A sphere of distinct electron density appears between N-7 of the purine base and the 5′-phosphoryl group of AMP in each of the symmetry unique subunits of the T-state complexes. Thermal parameters for water molecules refined here averaged to approximately 22 Å^2. In the crystal structure of an AMP complex of recombinant human FBPase, AMP binds to its allosteric pocket in the anti conformation with a water molecule between N-7 of the purine base and the 5′-phosphoryl group (*32*). In crystal structures of natural and recombinant pig kidney FBPase (the amino acid sequence of which is identical to that of recombinant porcine FBPase), the AMP molecule is present in an anti conformer, a syn conformer, or an equally weighted mixture of syn and anti conformers with no water molecule bridging the N-7 and 5′-phosphoryl groups (*16*, *17*, *31*). Reported instances of syn conformers may reflect the inherent difficulty of interpreting electron density from low-resolution diffraction data. Electron density from a water molecule near the N-7 atom could merge with the purine base of AMP, leading to the assignment of a syn conformer. Alternatively, the presence of a bridging water molecule between the purine base of AMP and its 5′-phosphoryl group may be sensitive to conditions of crystallization.

F6P binds to the active site as the β-anomer in both the Mg^{2+} and Zn^{2+} complexes, but only in the Mg^{2+} complex is the 1-OH group coordinated to the cation at site 1 (Figures 3 and 4). The coordination of the 1-OH group to the site 1 metal was not observed either in the R-state, Zn^{2+}−product complex (*23*) or in substrate−analogue complexes of FBPase (*20*). The significance of this coordination is discussed below. P_i binds to the putative 1-phosphoryl site of $F16P_2$, directly coordinating the divalent cation (either Mg^{2+} or Zn^{2+}) at metal site 1. P_i and F6P retain many of the hydrogen bonds and nonbonded contacts observed in the R-state, metal−product complexes. Metal cations, however, do not occupy sites 2 and 3 in the T-state complexes. Loop 52−72, which putatively mediates allosteric inhibition by AMP, is disordered. Asp68 of loop 52−72 no longer hydrogen bonds with Arg276, a residue important for catalysis (*33*). Asp74, an essential catalytic residue (*34*), is poorly ordered, and does not hydrogen bond with backbone amide 71. As the major difference in crystallization conditions for the R- and T-state complexes reported here is the concentration of AMP (either 0 or 5 mM, respectively), the displacement of loop 52−72 and metal cations from the active site must result from AMP ligation of the allosteric pocket.

Metal−Product Complexes of FBPase in the R-State. Loop 52−72 is in the engaged conformation (*23*) in each of the R-state complexes reported here. Even so, at least two significant differences exist between the Zn^{2+}−product and Mg^{2+}−product complexes. As noted previously for the Zn^{2+}−product complex (*23*), the 1-OH group of F6P is not in the proper orientation for a nucleophilic attack on the P_i molecule. In the Mg^{2+}−product complex, however, the 1-OH group coordinates directly to the metal at site 1, as it does in its T-state complex, and is positioned ideally with respect to the P_i molecule for a nucleophilic displacement reaction (Figure 5). The distance separating the 1-oxygen atom of F6P and the phosphorus atom of P_i is 2.9 Å (in the T-state, which has two subunits per asymmetric unit, the corresponding distances average to 3.2 ± 0.1 Å). Hence, unlike the Zn^{2+}−product complex, the Mg^{2+}−product complex should be catalytically viable, even in the crystalline state.

The second major difference between the R-state complexes regards metal binding to the active site. In the Zn^{2+}−product complex, divalent cations are present at full occu-

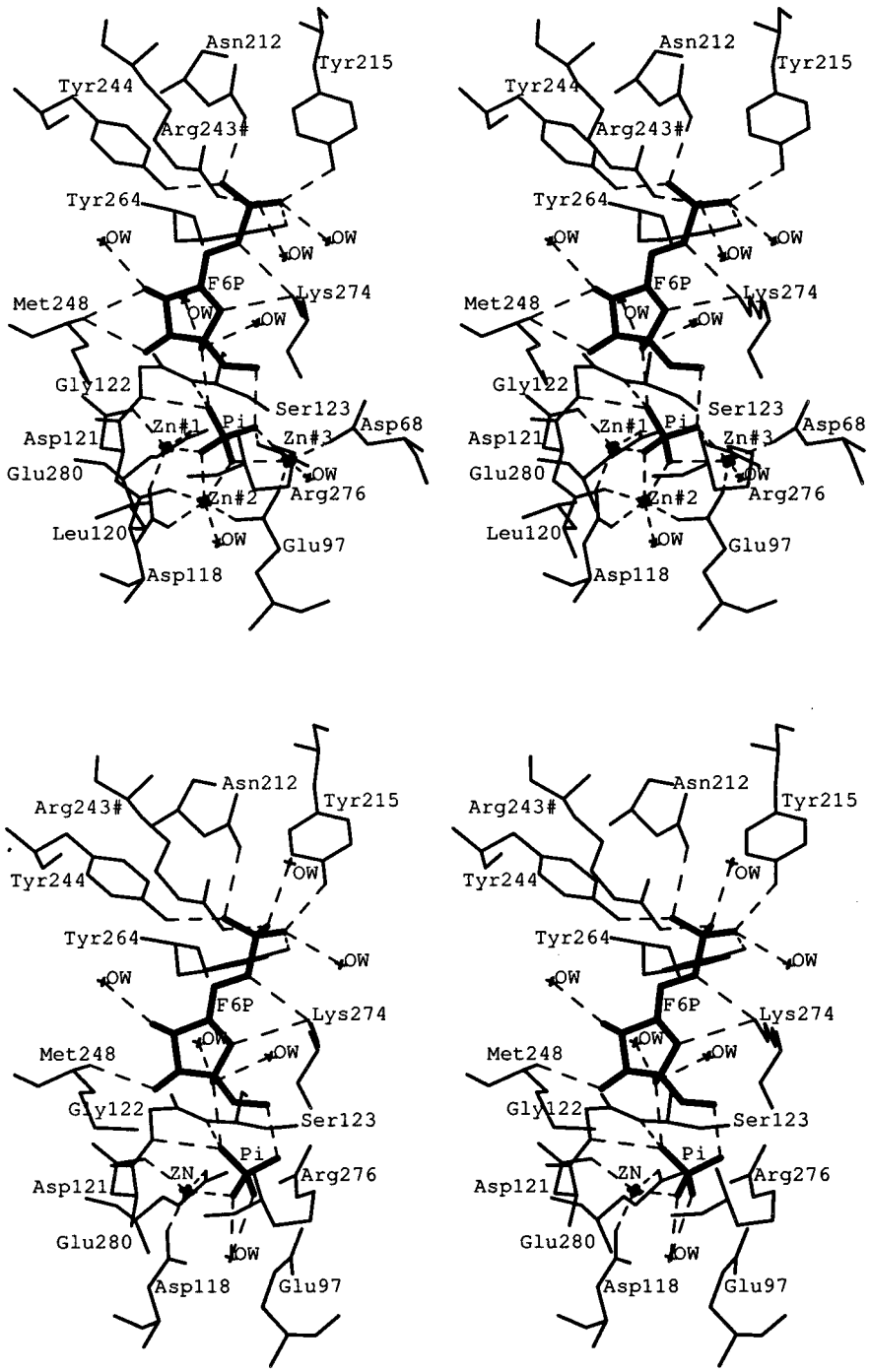

FIGURE 3: Stereoviews of the active site for T- and R-state, Zn^{2+}−product complexes. The R-state has three metal cations (top). The T-state has one metal cation at site 1 (bottom). Dashed lines represent donor−acceptor interactions or coordinate bonds. Bold lines represent ligands (F6P and P_i). The 1-OH group of F6P does not coordinate to the cation at site 1.

pancy at three sites (Figure 3). Metals at sites 1−3 coordinate directly to P_i at the 1-phosphoryl site of $F16P_2$. In the Mg^{2+}−product complex, however, divalent cations occupy sites 1 and 2, both of which coordinate to P_i (Figure 4). Electron density in the Mg^{2+}−product complex, which coincides with metal site 3 in the Zn^{2+}−product complex, appears as an extension of density from the P_i molecule (Figure 5). The electron density, here, could reflect the presence of Mg^{2+} at low occupancy, or be simply a noise artifact. A sphere of electron density, located approximately 2 Å away from the location of metal site 3 (as defined in the Zn^{2+}−product complex), however, could represent a water molecule or an alternative cation binding site (Figure 5). A water molecule, here, must bond exclusively as a proton donor and tolerate several nonbonded contacts involving oxygen atoms from the protein (Asn64, Asp68, Asp74, and Glu98) and/or the bound P_i molecule. Alternatively, the electron density could represent bound K^+ at low occupancy. On the basis of kinetics, the affinity constant for K^+ in the presence of 5 mM Mg^{2+} is approximately 25 mM, whereas the concentration of K^+ (present as a counterion of P_i) is 10 mM.

More subtle differences between the R-state Mg^{2+} and Zn^{2+} complexes extend beyond metal site 3 and the coordination of the 1-OH group of F6P by the metal at site 1. The conformations of Arg276 and Glu97 differ modestly in the two complexes. Ser123 hydrogen bonds with P_i in

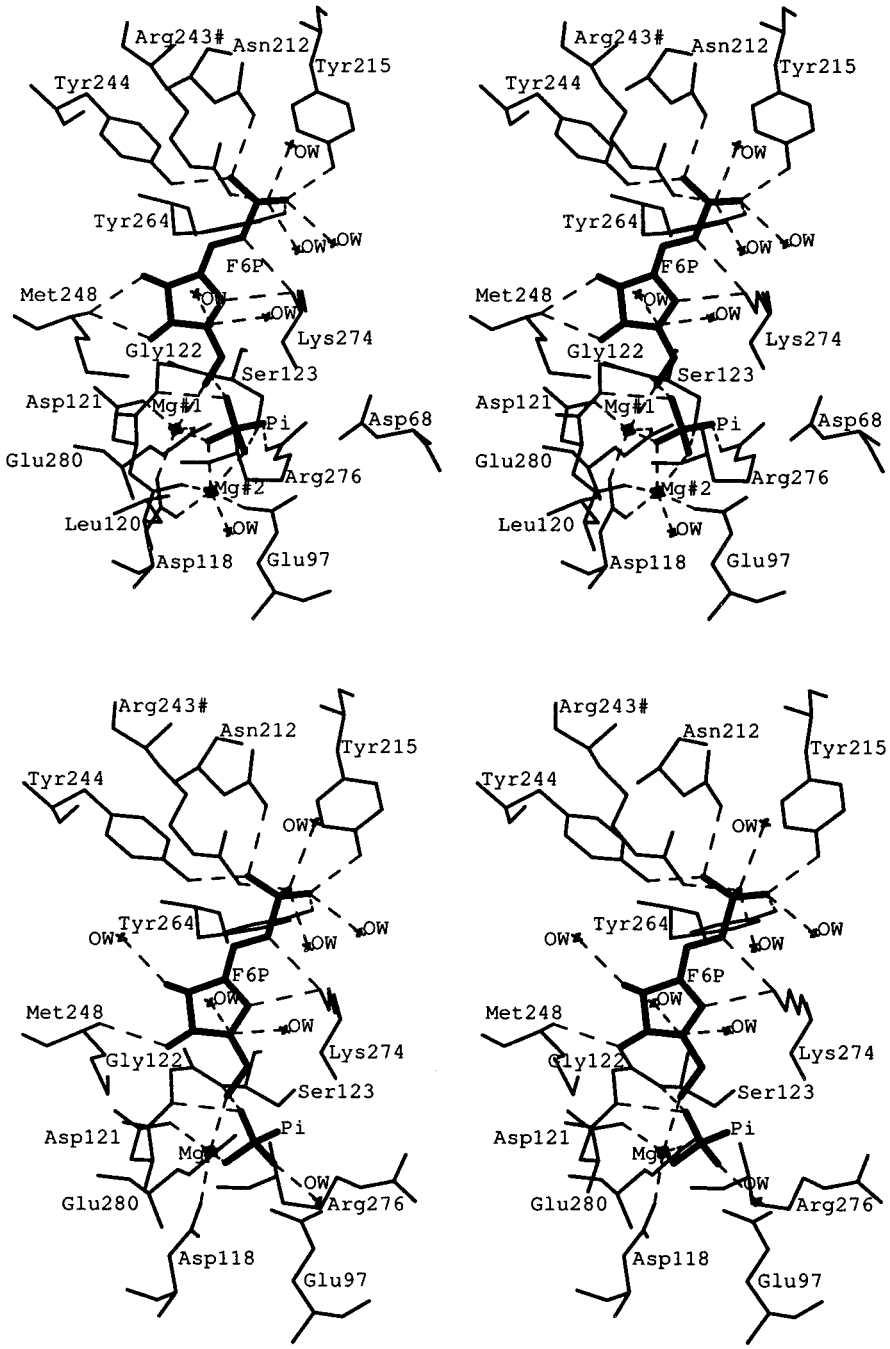

FIGURE 4: Stereoviews of the active site for T- and R-state, Mg^{2+}−product complexes. The R-state has two metal cations at sites 1 and 2 (top). The T-state has one metal cation at site 1 (bottom). Dashed lines represent donor−acceptor interactions or coordinate bonds. Bold lines represent ligands (F6P and P_i). The 1-OH group of F6P makes a coordinate bond to the Mg^{2+} at site 1.

the Mg^{2+}−product complex, and the side chain of Lys71 is in weak electron density; on the other hand, in the Zn^{2+}−product complex, Ser123 hydrogen bonds to the side chain of Lys71. Finally, the furanosyl moiety of F6P occupies positions differing by approximately 0.2 Å in the two R-state complexes. Alone, the differences described above could be attributed to coordinate uncertainty and/or an artifact of refinement; however, taken together, they probably represent real differences in the Mg^{2+}- and Zn^{2+}-coordinated active sites.

Even though site 3 is largely unoccupied by metal in the Mg^{2+}−product complex, the side chain of Asp68 and the bound P_i molecule are within 0.2 Å of their respective positions in the Zn^{2+}−product complex. In fact, the side chain of Asp68 and the P_i molecule may be at times hydrogen bonded to each other in the absence of metal (donor−acceptor distance of 3.4 Å). The significance of a shared proton between Asp68 and the P_i molecule is discussed below.

DISCUSSION

The structures presented here confirm the main features of a model for allosteric regulation of catalysis in FBPase proposed by Choe et al. (*23*). AMP alone displaces loop 52−72 from its engaged conformation and abolishes metal association with sites 2 and 3 (Figure 2). Studies in kinetics (*11*), fluorescence (*18*), and NMR (*19*) consistently reflect

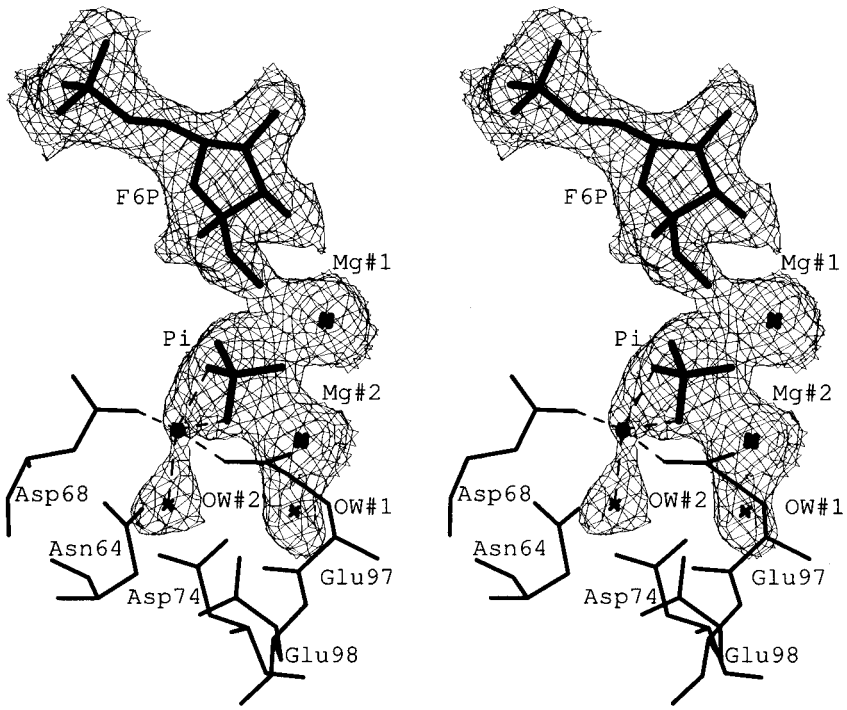

FIGURE 5: Stereoview of electron density from a $2F_{obs} - F_{calc}$ map covering active site ligands of the R-state, Mg^{2+}−product complex. The contour level is 1σ with a cover radius of 1.5 Å. The black dot represents the location of metal site 3 in the Zn^{2+}−product complex. Dashed lines indicate atoms proximal to this site, with distances varying from 2 to 2.5 Å. The density labeled OW#2 may be a water molecule or a K^+ at low occupancy.

competition in the binding of AMP and metal cations to FBPase. The work here confirms the mutually exclusive relationship between metal cation and AMP association with FBPase, at least in the presence of bound products. The structures implicate AMP in the release of metal cations only from sites 2 and 3. The metal cation is present at site 1 regardless of AMP ligation and the conformation of loop 52−72. Conceivably, metal cation affinity is reduced for site 1 in the T-state, but the conditions employed here (5 mM Mg^{2+} or 2 mM Zn^{2+}) do not permit a quantitative measure of binding affinities for cations.

Heretofore, we have considered only two conformational states for FBPase: disengaged loop, T-state or engaged loop, R-state. Loop 52−72 can be disengaged, however, in the R-state as well, especially in the absence of metal cations (*17*). The disengaged loop in the R-state is disordered entirely from residues 52 to 72, in contrast to the disengaged loop of the T-state, which is disordered only from residues 63 to 70. Hence, T-state FBPase selects a specific conformation for residues 52−62, which is incompatible with an engaged loop conformation. The key interactions here include nonbonded contacts between Ile10 of an adjacent subunit of the tetramer with residues 52−55 (Figure 6).

The binding of AMP to the allosteric effector site sets into motion a series of conformational changes, which transform FBPase from an engaged loop, R-state conformation to a disengaged loop, T-state conformation. The mechanism by which AMP promotes the R- to T-state transition has been analyzed by Zhang et al. (*15*). AMP triggers a conformational change in the connecting loop between helices H1 and H2, which in turn facilitates new interactions across the C1−C4 interface of the T-state (such as the hydrogen bond between Thr27 and Arg22). Evidently, the conformational response requires the entire AMP molecule, as the enzyme remains

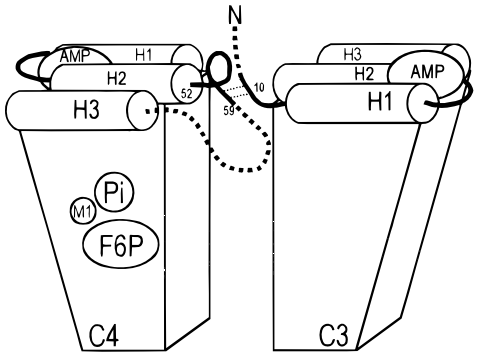

FIGURE 6: Schematic of the interaction between loop 52−72 and the N-terminal segment of an adjacent subunit. The orientation of the C3−C4 subunit pair is consistent with that of Figure 1.

in an R-state conformation, even though P_i saturates the binding site for the 5′-phosphoryl group of AMP.

The concentration of Mg^{2+} employed here is comparable to that used in assays of FBPase activity. The concentration of K^+ (approximately 10 mM), however, is well below the affinity constant for K^+ activation (25 mM), measured in the presence of 5 mM Mg^{2+}. We do not expect then appreciable levels of bound K^+ in the Mg^{2+}−product complex. As sites 1 and 2 are completely occupied by Mg^{2+}, whereas site 3 is virtually unoccupied, we tentatively regard site 3 as the locus for K^+ association. Other studies also implicate site 3 in monovalent cation activation. Chemical modification of an arginine abolishes K^+ activation (*35*). Arg276 and Arg313 are 3.9 and 8.3 Å, respectively, from metal site 3. T-State crystals, grown in the presence of 500 mM KCl, reveal three K^+ binding sites (*30*), which superimpose approximately on the three metal sites reported here in R-state product complexes. Mutations, which destabilize an engaged loop 52−72, also abolish K^+ activation and

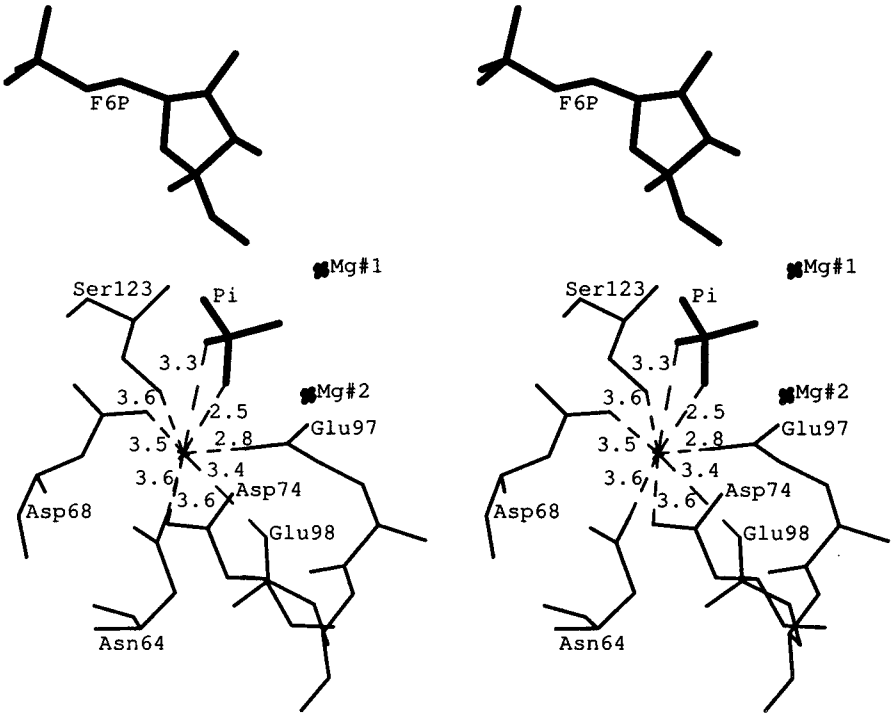

FIGURE 7: Model for the K^+-ligated active site of FBPase in the R-state. K^+ can interact with several oxygen atoms, but the means by which it enhances catalysis is uncertain.

increase the Mg^{2+} affinity constant (S. Nelson, J.-Y. Choe, R. B. Honzatko, and H. J. Fromm, unpublished observations). Of the three metal sites, loop 52−72 interacts directly with the cation at site 3 only.

The zinc cation binds to site 3 at a concentration of 5 mM in R-state, product complexes, perhaps due to its high affinity for P_i relative to that of Mg^{2+} and K^+. Mg^{2+} may also bind to site 3 at concentrations of >5 mM, but in kinetic assays, such levels of magnesium cation cause inhibition. Indeed, Zn^{2+} is nearly as effective as Mg^{2+} in supporting FBPase catalysis, but at the high concentration of zinc used here, enzyme activity is well below its optimal level (J.-Y. Choe, H. J. Fromm, and R. B. Honzatko, unpublished observations). Inhibition of FBPase at high Mg^{2+} and Zn^{2+} concentrations may originate in part from the binding of metal cation to site 3, as observed in the Zn^{2+}−product complex. A cation at site 3 could impair a proton-transfer step in the catalytic mechanism, as discussed below.

If a metal at site 3 is indeed inhibitory, then from which site does potassium enhance FBPase activity? K^+ could coordinate oxygen atoms from P_i, Asn64, Asp68, Asp74, and/or Glu98 (Figure 7). In the Mg^{2+}−product complex, electron density at this site, tentatively assigned to a water molecule, can support two hydrogen bonds (three hydrogen bonds in the case of a hydronium ion). K^+ can support more interactions than a water molecule, and could stabilize an active site with a superior arrangement of functional groups. We emphasize here, however, that this proposed site of K^+ interaction is not identical to metal site 3 of the Zn^{2+}−product complex. Small cations, such as Li^+ and Zn^{2+}, may bind to metal site 3 and cause inhibition, whereas large cations (K^+, NH_4^+, and Tl^+), which enhance catalysis, may bind to the more spacious site in place of the observed water molecule. Product complexes of FBPase, cocrystallized with Mg^{2+} and monovalent cations under conditions similar to those used

Table 2: Selected Distances to Metal Ions and P_i in Product Complexes of FBPase

	distance (Å)			
interaction	R-state Zn^{2+}	R-state Mg^{2+}	T-state Zn^{2+}	T-state Mg^{2+}
metal site 1				
P_i O2	2.01	2.00	2.14	1.98
Asp118 OD1	1.88	2.23	2.27	2.07
Asp121 OD1	2.17	1.90	1.87	2.08
Glu280 OE1	2.07	2.08	2.19	2.08
F6P O1	4.99	2.28	4.73	2.29
metal site 2				
P_i O2	2.35	2.31		
P_i O3	2.20	2.37		
Glu97 OE1	1.95	2.24		
Asp118 OD2	2.14	2.09		
Leu120 O	2.35	2.06		
water	2.28	2.17		
metal site 3				
P_i O3	2.47			
P_i O1	2.14			
Asp68 OD2	2.38			
Glu97 OE2	2.38			
P_i O1[a]				
F6P O1	2.68	3.05	2.62	2.82
Arg276 NH2	2.92	2.72	3.17	6.80
Asp68 OD2	3.20	3.37	18.26	18.67
Glu97 OE1	3.93	3.44	3.20	3.22
P_i O2[a]				
Glu97	3.13	3.28		
Arg276	3.45	3.58	3.11	8.69
water			3.15	
P_i O3[a]				
Ser123 OG	4.43	2.80	4.13	3.43
water			2.77	2.87
P_i O4				
F6P O2	2.63	3.33	2.78	3.40
Gly122 N	2.91	3.04	3.02	2.73
Gly123 N	2.86	2.83	3.00	2.67

[a] Does not include coordination to metal sites listed above in the table.

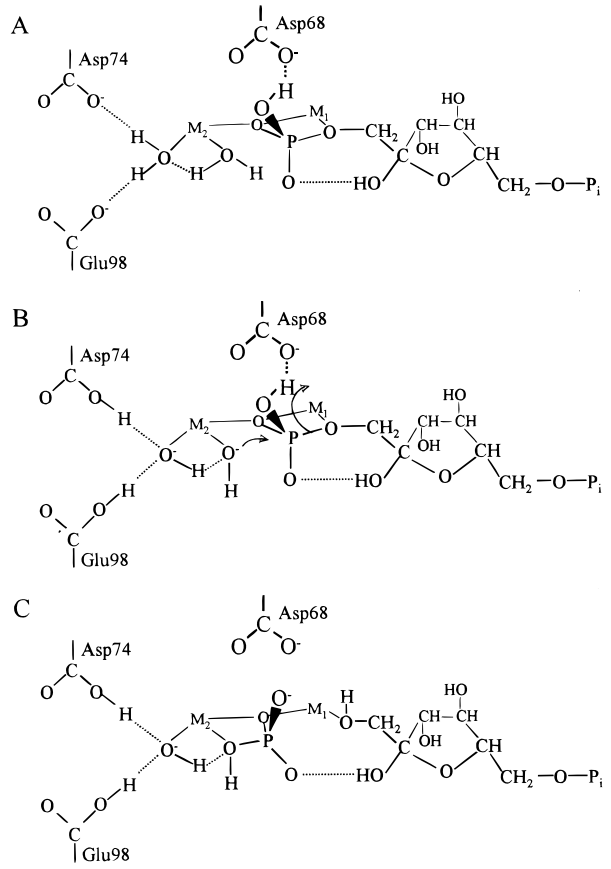

FIGURE 8: Mechanism for the hydrolysis of $F16P_2$, derived from the R-state, Mg^{2+}−product complex: (A) F16P2 complex, (B) transition state, and (C) product complex. See the text for further explanation.

in kinetic assays, may further clarify the role of the third metal site in the catalytic mechanism of FBPase.

The direct coordination of the 1-OH group of F6P to the Mg^{2+} at site 1 implicates that metal cation in the catalytic mechanism of FBPase. In contrast, Zn^{2+} at site 1, perhaps because of its small ionic radius relative to Mg^{2+}, may not easily accept the 1-OH group of F6P as a fifth coordinating ligand. Mg^{2+} at site 1 probably stabilizes the development of negative charge on the 1-oxygen atom of $F16P_2$ in the forward reaction and the same atom of F6P in the reverse reaction. Hence, the metal at site 1 in productive complexes may be five-coordinate. The Mg^{2+} at metal site 2, however, is six-coordinate (Table 2), and probably has two water molecules in its inner sphere at the onset of the forward reaction (Figure 8). Asp74 and Glu98, both essential to catalysis at pH 7.5 (*34*, *37*), hydrogen bond to one of two water molecules coordinated to the Mg^{2+} at site 2. That water molecule acts as a catalytic base in the abstraction of a proton from the second coordinated water molecule (which could be a hydroxide ion at higher pH). The resulting hydroxide anion is the attacking nucleophile in the displacement of F6P. Charge on the 1-oxygen atom of F6P is stabilized by its coordination to the Mg^{2+} at site 1. In addition, we suggest the presence of a proton on the 1-phosphoryl group of $F16P_2$, shared in a hydrogen bond with Asp68 prior to the start of the reaction, which moves to the 1-oxygen atom of F6P late in the transition state. Hence, a small cation (such as Mg^{2+}, Zn^{2+}, or Li^+), interacting with the 1-phosphoryl group and Asp68, as observed in the Zn^{2+}−product complex, would displace this proton and impair the mechanism of proton transfer. The role of the monovalent cation, then, may be to maintain Asp68 in proximity to the 1-phosphoryl group of $F16P_2$, without directly coordinating either functional group.

REFERENCES

1. Krebs, H. A. (1963) in *Advances in Enzyme Regulation* (Weber, G., Ed.) Vol. 1, pp 385−400, Pergamon Press Ltd., London.
2. Marcus, F. (1981) in *The Regulation of Carbohydrate Formation and Utilization in Mammals* (Veneziabe, C. M., Ed.) pp 269−290, University Park Press, Baltimore.
3. Benkovic, S. J., and de Maine, M. M. (1982) *Adv. Enzymol. Relat. Areas Mol. Biol. 53*, 45−82.
4. Hers, H. G., and Hue, L. (1983) *Annu. Rev. Biochem. 52*, 617−653.
5. Tejwani, G. A. (1983*) Adv. Enzymol. Relat. Areas Mol. Biol. 54*, 121−194.
6. Pilkus, S. J., El-Maghrabi, M. R., and Claus, T. H. (1988) *Annu. Rev. Biochem. 57*, 755−783.
7. Taketa, K., and Pogell, B. M. (1965*) J. Biol. Chem. 240*, 651−662.
8. Nimmo, H. G., and Tipton, K. F. (1975*) Eur. J. Biochem. 58*, 567−574.
9. Stone, S. R., and Fromm, H. J. (1980) *Biochemistry 19*, 620−625.
10. McGrane, M. M., El-Maghrabi, M. R., and Pilkus, S. J. (1983) *J. Biol. Chem. 258*, 10445−10454.
11. Liu, F., and Fromm, H. J. (1988) *J. Biol. Chem. 263*, 9122−9128.
12. Sola, M. M., Oliver, F. J., Salto, R., Gutierrez, M., and Vargas, A. M. (1993) *Int. J. Biochem. 25*, 1963−1968.
13. Zhang, R., Villeret, V., Lipscomb, W. N., and Fromm, H. J. (1996) *Biochemistry 35*, 3038−3043.
14. Nimmo, H. G., and Tipton, K. F. (1975) *Eur. J. Biochem. 58*, 575−585.
15. Zhang, Y., Liang, J.-Y., Huang, S., and Lipscomb, W. N. (1994) *J. Mol. Biol. 244*, 609−624.
16. Ke, H., Zhang, Y., and Lipscomb, W. N. (1990) *Proc. Natl. Acad. Sci. U.S.A. 87*, 5243−5247.
17. Ke, H., Zhang, Y., Liang, J.-Y., and Lipscomb, W. N. (1991) *Proc. Natl. Acad. Sci. U.S.A. 88*, 2989−2993.
18. Scheffler, J. E., and Fromm, H. J. (1986) *Biochemistry 25*, 6659−6665.
19. Liu, F., and Fromm, H. J. (1990) *J. Biol. Chem. 265*, 7401−7406.
20. Zhang, Y., Liang, J.-Y., Huang, S., Ke, H., and Lipscomb, W. N. (1993) *Biochemistry 32*, 1844−1857.
21. Xue, Y., Huang, S., Liang, J.-Y., Zhang, Y., and Lipscomb, W. N. (1994) *Proc. Natl. Acad. Sci. U.S.A. 91*, 12482−12486.
22. Villeret, V., Huang, S., Zhang, Y., and Lipscomb, W. N. (1995) *Biochemistry 34*, 4307−4315.
23. Choe, J.-Y., Poland, B. W., Fromm, H. J., and Honzatko, R. B. (1998) *Biochemistry 37*, 11441−11450.
24. Burton, V. A., Chen, M., Ong, W. C., Ling, T., Fromm, H. J., and Stayton, M. M. (1993) *Biochem. Biophys. Res. Commun. 192*, 511−517.
25. Howard, A. J., Nielsen, C., and Xuong, N. H. (1985) *Methods Enzymol. 114*, 452−472.
26. McRee, D. E. (1992*) J. Mol. Graphics 10*, 44−46.
27. Brünger, A. T., Adams, P. D., Clore, G. M., DeLano, W. L., Gros, P., Grosse-Kunstleve, R. W., Jiang, J.-S., Kuszewski, J., Nilges, M., Pannu, M. S., Read, R. J., Rice, L. M., Simonson, T., and Warren, G. L. (1998) *Acta Crystallogr., Sect. D 54*, 905−921.
28. Engh, R. A., and Huber, R. (1991) *Acta Crystallogr., Sect. A 47*, 392−400.
29. Laskowski, R. A., MacArthur, M. W., Moss, D. S., and Thornton, J. M. (1993) *J. Appl. Crystallogr. 26*, 283−291.
30. Villeret, V., Huang, S., Fromm, H. J., and Lipscomb, W. N. (1995) *Proc. Natl. Acad. Sci. U.S.A. 92*, 8916−8920.
31. Stec, B., Abraham, R., Giroux, E., and Kantrowitz, E. R. (1996) *Protein Sci. 5*, 1541−1553.

32. Iversen, L. F., Brzozowski, M., Hastrup, S., Hubbard, R., Kastrup, J. S., Larsen, I. K., Nærum, L., Nørskov-Lauridsen, L., Rasmussen, P. B., Thim, L., Wiberg, F. C., and Lundgren, K. (1997) *Protein Sci. 6*, 971−982.
33. Zhang, R., and Fromm, H. J. (1995) *Biochemistry 34*, 8190−8195.
34. Kurbanov, F. T., Choe, J.-Y., Honzatko, R. B., and Fromm, H. J. (1998) *J. Biol. Chem. 273*, 17511−17516.
35. Marcus, F. (1975) *Biochemistry 14*, 3916−3921.
36. Zhang, R., Villeret, V., Lipscomb, W. N., and Fromm, H. J. (1996) *Biochemistry 35*, 3038−3043.
37. Kelly, N., Giroux, E. L., Lu, G., and Kantrowitz, E. R. (1996) *Biochem. Biophys. Res. Commun. 219*, 848−852.
38. Merritt, E. A., and Bacon, D. J. (1997) *Methods Enzymol. 277*, 505−524.
39. Kraulis, J. (1991) *J. Appl. Crystallgr. 24*, 946−950.

BI000574G